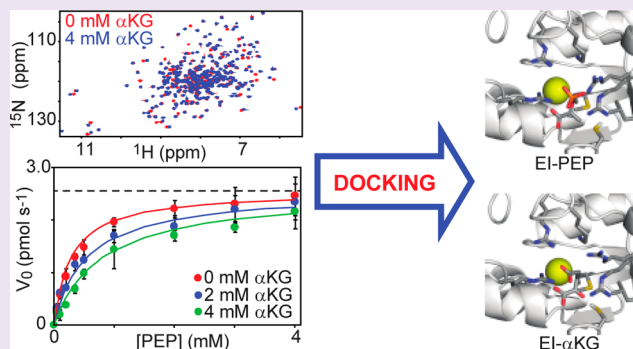


Structural Basis for Enzyme I Inhibition by α -KetoglutarateVincenzo Venditti,[†] Rodolfo Ghirlando,[‡] and G. Marius Clore^{*,†}[†]Laboratories of Chemical Physics and [‡]Molecular Biology, National Institute of Diabetes and Digestive and Kidney Diseases, National Institutes of Health, Bethesda, Maryland 20892-0520, United States

S Supporting Information

ABSTRACT: Creating new bacterial strains in which carbon and nitrogen metabolism are uncoupled is potentially very useful for optimizing yields of microbial produced chemicals from renewable carbon sources. However, the mechanisms that balance carbon and nitrogen consumption in bacteria are poorly understood. Recently, α -ketoglutarate (α KG), the carbon substrate for ammonia assimilation, has been observed to inhibit *Escherichia coli* enzyme I (EI), the first component of the bacterial phosphotransferase system (PTS), thereby providing a direct biochemical link between central carbon and nitrogen metabolism. Here we investigate the EI- α KG interaction by NMR and enzymatic assays. We show that α KG binds with a K_D of ~ 2.2 mM at the active site of EI, acting as a competitive inhibitor. In addition, we use molecular docking simulations to derive a structural model of the enzyme–inhibitor complex that is fully consistent with NMR and analytical ultracentrifugation data. We expect that the EI- α KG structure presented here will provide a starting point for structure-based design of EI mutants resistant to α KG.



Investigating the mechanisms by which cells integrate information from multiple intra- and extracellular nutrient-sensing pathways is an important aspect of modern biochemistry. In humans, undesired metabolic imbalances can lead to obesity, diabetes, and cancer.^{1,2} In bacteria, efficient reprogramming of metabolic pathways can be exploited to produce valuable products, including biodegradable plastics³ and biofuels.^{4–6}

A major contribution to this area of research has recently been provided by Doucette et al.,⁷ who showed that α -ketoglutarate (α KG), the carbon substrate for ammonia assimilation that accumulates in *E. coli* (as well as in other prokaryotic and eukaryotic cells⁸) under conditions of nitrogen limitation, directly blocks glucose uptake across the bacterial membrane by inhibition of enzyme I (EI). Autophosphorylation of EI by phosphoenolpyruvate (PEP) is the first step in the bacterial phosphoenolpyruvate:sugar phosphotransferase system (PTS), a signal transduction pathway in which phosphoryl transfer via a series of bimolecular protein–protein interactions is coupled to active transport of sugars across the membrane.⁹ Inhibition of EI by α KG therefore provides a direct regulatory link between central carbon and nitrogen metabolism in *E. coli* and represents one of the few documented biochemical mechanisms to date whereby bacterial cells regulate the transport of one elemental nutrient in response to the availability of another. Thus, obtaining structural insights into the inhibition of EI by α KG may serve as a model for more complex cases relevant to eukaryotic biology and may provide the basis for engineering new bacterial strains in which carbon and nitrogen metabolism are uncoupled. Such strains may be

helpful for maximizing the efficiency of microbial overproduction of bioderived molecules where conditions of nitrogen limitation are used to force carbon metabolism into nonphysiological pathways.^{10–12}

Here we present the structural characterization of the EI- α KG interaction. Using biochemical assays and NMR titration experiments, we demonstrate that α KG and PEP compete for the same binding site on the C-terminal domain of EI. On the basis of these results, we use molecular docking simulations to propose a structural model for the EI- α KG complex that is in perfect agreement with the effects of α KG on the NMR spectra and sedimentation properties of EI.

RESULTS AND DISCUSSION

NMR Spectroscopy. The functional form of EI is a ~ 128 kDa dimer of identical subunits comprising two structurally and functionally distinct domains connected to one another by a long helical linker.¹³ The N-terminal domain (EIN, residues 1–249) contains the site of phosphorylation (His¹⁸⁹). The C-terminal domain (EIC, residues 261–575) is responsible for dimerization and contains the binding site for PEP. We have investigated the interaction of α KG with the isolated EIN and EIC domains by NMR spectroscopy, and the results are summarized in Figure 1. Addition of 4 mM α KG to the protein samples does not alter the ¹H-¹⁵N TROSY spectrum of EIN (Figure 1a) but results in substantial changes in the EIC

Received: January 11, 2013

Accepted: March 18, 2013

Published: March 18, 2013

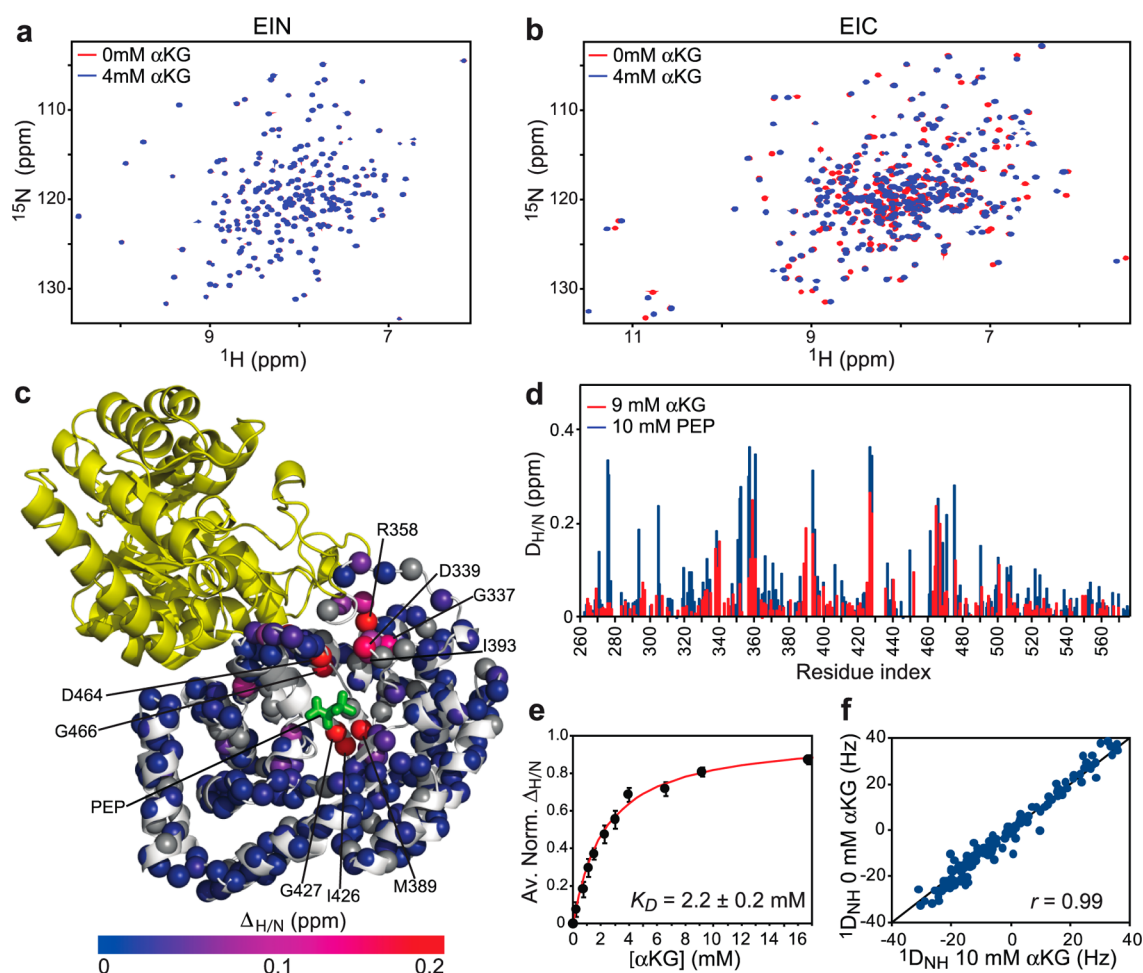


Figure 1. NMR characterization of the EI- α KG interaction. 600 MHz ^1H - ^{15}N TROSY spectra of (a) EIN and (b) EIC acquired in the absence (red) and presence (blue) of 4 mM α KG. (c) Structural model for the EIC-PEP complex¹⁴ showing the extent of $^1\text{H}/^{15}\text{N}$ chemical shift perturbation ($\Delta_{\text{H}/\text{N}}$) upon addition of 9 mM α KG to the protein sample. Assigned backbone amides are depicted as spheres and colored according to their $\Delta_{\text{H}/\text{N}}$ values (color bar ranging from blue to red). Amide groups assigned only for free EIC are displayed as gray spheres. PEP is indicated as green bonds. The two subunits of the EIC dimer are colored in white and yellow. (d) Comparison of the $\Delta_{\text{H}/\text{N}}$ profiles obtained for EIC in the presence of 9 mM α KG (red) and 10 mM PEP¹⁴ (blue). (e) $\Delta_{\text{H}/\text{N}}$ values as a function of the α KG concentration. Data for all residues showing $\Delta_{\text{H}/\text{N}} > 0.1$ ppm at 16 mM α KG were simultaneously fit (red curve) using a one-site binding model (see Methods) yielding a K_{D} value of $2.2 (\pm 0.2)$ mM. In the figure, the $\Delta_{\text{H}/\text{N}}$ were normalized with respect to the fitted $\Delta_{\text{H}/\text{N}}$ at saturation and averaged over all of the residues used in the fitting procedure. The error bars are set to one standard deviation. (f) Correlation between the backbone amide RDCs ($^1\text{D}_{\text{NH}}$) measured for EIC in the absence and presence of 10 mM α KG. The high degree of correlation indicates that the orientation of backbone amide bond vectors relative to the external alignment tensor is unchanged in the two samples, showing that binding of α KG does not result in any significant change in backbone conformation.

spectrum (Figure 1b), indicating that the EI- α KG interaction occurs exclusively within the C-terminal domain. Analysis of the $^1\text{H}_{\text{N}}/^{15}\text{N}$ chemical shift perturbation ($\Delta_{\text{H}/\text{N}}$) profile generated by the inhibitor on the combined $^1\text{H}_{\text{N}}/^{15}\text{N}$ chemical shifts of EIC yields an equilibrium dissociation constant (K_{D}) of $\sim 2.2 \pm 0.2$ mM for the EI- α KG complex (Figure 1e), which is ~ 6 times larger than the K_{m} reported for the EIC-PEP interaction (~ 0.35 mM¹⁴). The $\Delta_{\text{H}/\text{N}}$ profiles at near-saturating concentrations of PEP and α KG are very similar (Figure 1d) with α KG inducing the largest chemical shift perturbations at the binding site for PEP (Figure 1c). These data suggest that PEP and α KG compete for the same binding site on EIC, in contrast with the previously reported non-competitive mechanism proposed for EI inhibition by α KG.⁷

Inhibition Assay. To investigate whether α KG affects the stability of the EIC-PEP complex, the ability of EIC to hydrolyze PEP¹⁴ was assayed in the presence of 0, 2, and 4 mM α KG. The resulting kinetic data are reported in Figure 2 and

indicate that α KG efficiently inhibits the hydrolytic activity of the enzyme. Fitting the enzymatic data to a competitive inhibition model (eq 3) yields a K_{m} of 0.3 ± 0.1 mM and a K_{I} of 2.2 ± 0.5 mM (Figure 2a), which are in excellent agreement with the K_{m} value previously reported for the EIC-PEP interaction¹⁴ and with the K_{D} for the EIC- α KG complex obtained by NMR titration experiments (this work), respectively. In contrast, a much poorer fit is obtained when a non-competitive inhibition model (eq 4) is used to interpret the enzymatic data (Figure 2b), confirming that formation of the EIC- α KG complex disrupts the interaction of EI with PEP.

The K_{m} and K_{I} values (0.3 and 2.2 mM, respectively), which correspond to the equilibrium dissociation constants for the EIC-PEP and EIC- α KG complexes, respectively, were used to calculate the effect of increasing concentrations of α KG on the EI-PEP complex at physiological concentrations of enzyme, substrate, and inhibitor. This simulation reveals that 4 mM α KG is sufficient to reduce the percentage of intracellular EI

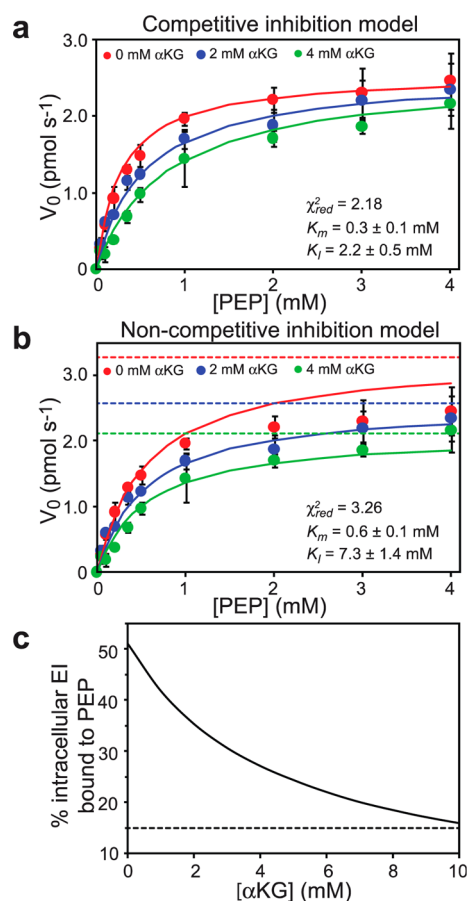


Figure 2. Competitive inhibition of EI by α KG. Michaelis–Menten kinetics for EIC with the substrate PEP. Enzymatic assays were performed in the presence of 0 (red), 2 (blue), and 4 (green) mM α KG. The kinetic data were fitted using competitive (a) and non-competitive (b) inhibition models. (c) Simulation of the percentage of intracellular EI bound to PEP at different concentration of α KG (see Methods).

bound to PEP from $\sim 50\%$ to $\sim 25\%$ (Figure 2c), and this value becomes even lower ($\sim 15\%$) when the concentration of α KG reaches 10 mM (which corresponds to the intracellular concentration of α KG measured in *E. coli* cultures grown under nitrogen-poor conditions⁷).

Docking Simulations. Taken together, the chemical shift perturbation and enzymatic assay data clearly indicate that PEP and α KG compete for the same binding site on EIC. In addition, the backbone amide (¹D_{NH}) residual dipolar couplings (RDCs) measured on samples of weakly aligned EIC and EIC- α KG complex are highly correlated (Figure 1f), indicating the absence of any significant α KG-induced conformational rearrangements in EIC that could result in allosteric disruption of the EIC-PEP interaction. Thus, a structure for the EIC- α KG complex can be obtained by molecular docking of an α KG molecule into the EIC binding site for PEP. Docking simulations with AutoDock 4.0³³ were performed as described in Methods, and the resulting EIC- α KG complex is compared to the EIC-PEP structure in Figure 3. As expected from the close similarity of the chemical structures of the two molecules (Figure 3a), docking results show that PEP and α KG adopt a similar binding mode on EIC. Indeed, for both ligands, the C¹ carboxylic group is involved in hydrogen-bonding interactions with the backbone amides of Asn⁴⁵⁴ and Asp⁴⁵⁵ (Figure 3b,c),

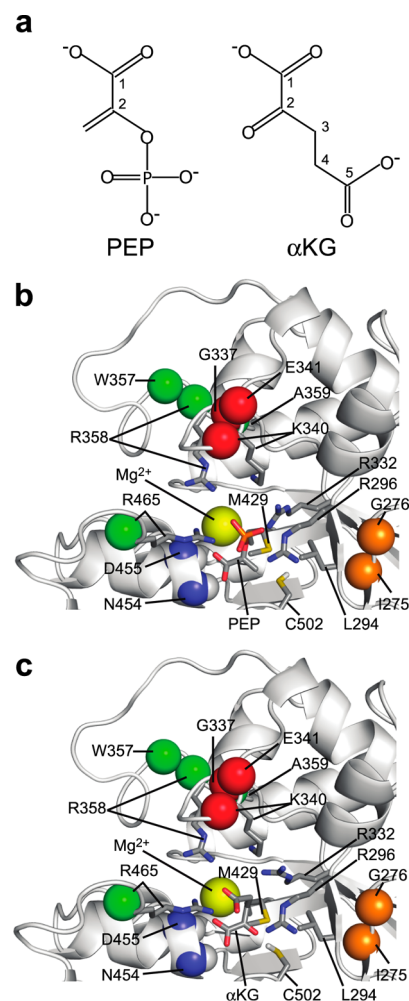


Figure 3. Comparison of PEP and α KG bound in the EIC active site. (a) Chemical structures of PEP and α KG. (b, c) Close up views of the EIC active site with bound PEP and α KG, respectively. The Mg²⁺ ion is shown as a yellow sphere. The amide groups of Asn⁴⁵⁴ and Asp⁴⁵⁵ are shown as spheres (blue, nitrogen; white, hydrogen). Side chains interacting with PEP and α KG are shown as bonds. The H γ proton of Cys⁵⁰² is indicated in white to highlight formation of a hydrogen bond with the carbonyl group of α KG. The amide groups of Ile²⁷⁵ and Gly²⁷⁶ are shown as orange spheres. Amide groups for which $|(\Delta\omega_N| - \Delta\delta_N)|/|\Delta\omega_N| > 0.5$ (see Table 1) are shown as red spheres (Gly³³⁷, Lys³⁴⁰, Glu³⁴¹). Amide groups for which $|(\Delta\omega_N| - \Delta\delta_N)|/|\Delta\omega_N| < 0.5$ (see Table 1) are shown as green spheres (Trp³⁵⁷, Arg³⁵⁸, Ala³⁵⁹, Arg⁴⁶⁵).

while the carbonyl group and the C⁵ carboxylic functionality of α KG perfectly overlap with the ethene and phosphoryl groups of PEP, respectively (Figure 3b,c). Interestingly, the docking results also indicate that although the carbonyl group of α KG is inserted in a small hydrophobic pocket formed by the Leu²⁹⁴ and Cys⁵⁰² side chains that accommodates the PEP ethene group in the EI-PEP complex (Figure 3b,c), the hydrophobic penalty engendered by substitution of the CH₂ group by the more polar O atom is compensated by formation of a hydrogen bond between the carbonylic oxygen of α KG and the thiol group of Cys⁵⁰² (Figure 3c). Thus the lower stability of the EI- α KG complex relative to that of EI-PEP must be primarily due to the looser interactions of the α KG C⁵ carboxyl group with the side chains of Arg²⁹⁶, Arg³³², Lys³⁴⁰, Arg³⁵⁸, and Arg⁴⁶⁵ (Figure 3c) that are involved in several hydrogen bonds and salt

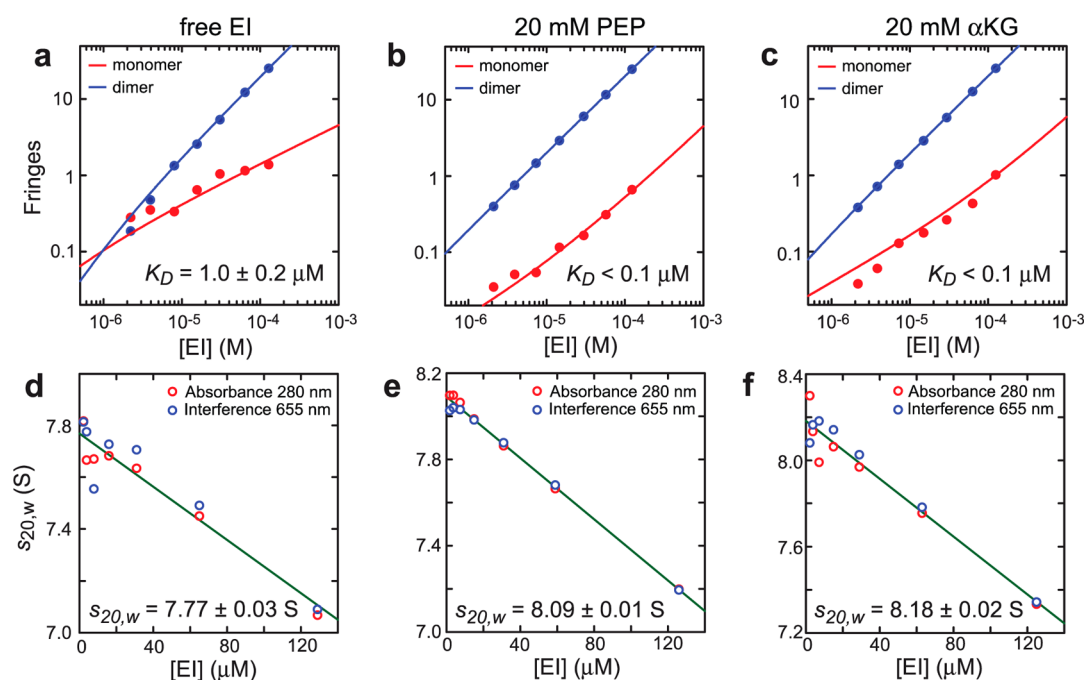


Figure 4. Effect of PEP and α KG on the monomer/dimer equilibrium of EI. (a–c) Population isotherms based on sedimentation velocity interference data (Supporting Information, Figure S1) showing the contributions of the EI monomer (red) and dimer (blue). All signals were normalized to a cell path length of 12 mm. The best fit monomer–dimer equilibrium analysis is depicted by the solid lines. For free EI (a) a K_D of $1.0 \pm 0.2 \mu\text{M}$ is obtained, consistent with previous reports.²² In the presence of 20 mM PEP (b) and 20 mM α KG (c), only traces of monomeric species are detected (Supporting Information, Figure S1). However, the sedimentation velocity data reported in panels b and c can be fit only by assuming that 2.0% of the monomer is incompetent for dimerization, indicating that the monomeric signals detected in panels b and c are due to small amounts of misfolded EI and/or other contaminants. Therefore, in the presence of PEP and α KG EI is essentially entirely dimeric ($K_D < 0.1 \mu\text{M}$). (d–f) Concentration dependence of the EI dimer weight-average sedimentation coefficients obtained from the $c(s)$ profiles. S -values at zero concentration were obtained from linear regression and extrapolation to zero concentration. Sedimentation coefficients of 7.77 ± 0.03 , 8.09 ± 0.01 , and $8.18 \pm 0.02 \text{ S}$ were determined for the EI dimer in the absence of ligands (d) and in the presence of 20 mM PEP (e) and 20 mM α KG (f), respectively, indicating that the ligand-bound structure of EI is more compact than the structure of the free enzyme and that the α KG-bound form is essentially as compact as the PEP-bound form.

bridges with the PEP phosphoryl group (Figure 3b). In particular, our model shows that the C⁵ carboxyl group of α KG forms two hydrogen bonds with Arg⁴⁶⁵ and is involved in electrostatic interactions with Arg³⁵⁸. In contrast to PEP, however, α KG makes only minor contacts with Arg²⁹⁶ and Lys³⁴⁰ and does not interact with the side chain of Arg³³².

Validation of the EI- α KG Structure. To validate the EI- α KG model obtained by molecular docking simulations, sedimentation velocity experiments were conducted on uniformly ²H/¹⁵N-labeled EI in the absence and presence of saturating concentrations of PEP and α KG. As previously reported, the specific network of interactions between EI and PEP induces structural stabilization of the EI dimer as well as a $\sim 70^\circ$ reorientation of EIN domain relative to EIC that results in a more compact enzyme structure.^{13–15} The sedimentation velocity data reported in Figure 4 reveal that addition of 20 mM PEP or α KG to EI results in a decrease of the EI dimer dissociation constant by more than an order of magnitude (Figure 4a–c) as well as in a corresponding increase in the sedimentation coefficient extrapolated for the EI dimer ($s_{20,w}$, Figure 4d,e). In particular, $s_{20,w}$ values of 7.77 ± 0.03 , 8.09 ± 0.01 , and $8.18 \pm 0.02 \text{ S}$ were obtained for the EI dimer in the free form and bound to PEP and α KG, respectively, indicating that the PEP-bound structure of EI is more compact than the structure of the free enzyme and that the α KG-bound form is essentially as compact as the PEP-bound form. The fact that PEP and α KG have similar effects on both the dimerization

properties and the overall shape of EI suggests that the two molecules share a common network of interactions with the enzyme, which is consistent with our model for the EI- α KG complex (Figure 3b,c).

We also noticed that the C⁵ carboxyl group of α KG is not a good analogue of the PEP phosphoryl group, which has a spherically distributed $-2e$ charge and is able to form electrostatic interactions with the Mg²⁺ ion and all of the positively charged side chains in the EIC active site. Indeed, the C⁵ carboxyl group of α KG bears an asymmetric $-1e$ charge and is preferentially oriented toward Arg⁴⁶⁵ in our model of the EIC- α KG complex, reproducing only the interactions of PEP with Arg³⁵⁸, Arg⁴⁶⁵ and the Mg²⁺ ion. To verify the existence of this preferential orientation, we compared the NMR data obtained for the EIC- α KG interaction with those previously reported for the EIC-PEP complex.¹⁴ NMR chemical shifts are sensitive reporters of the electronic environment surrounding a particular nucleus. Therefore, the observation of a nucleus with similar chemical shifts under different experimental conditions (i.e., in the absence of ligands, in the presence of PEP or α KG) indicates that the local environment surrounding the particular nucleus is unchanged. A perturbation in chemical shift, on the other hand, upon ligand binding is indicative of a change in chemical environment and can be used to reliably identify the site of interaction. Using this basic principle and NMR relaxation dispersion measurements, we have recently shown that the EIC residues around the PEP binding site undergo a

Table 1. Comparison between Chemical Shift Parameters ($\Delta\omega_N$) for the Open/Closed Conformational Exchange of EIC Obtained by NMR Relaxation Dispersion Experiments¹⁴ and ¹⁵N Chemical Shift Perturbations ($\Delta\delta_N$) Induced by α KG on the NMR Spectrum of EIC

	G337	K340	E341	L355	W357	R358	A359	I426	G427	R465	N467
$ \Delta\omega_N $ (ppm) ^a	2.0	0.6	1.0	1.1	1.0	0.7	2.0	1.9	2.0	0.8	0.8
$\Delta\delta_N$ (ppm)	0.6	0.1	0.4		0.7	0.9	1.1	1.6	1.5	1.0	
$ \Delta\omega_N - \Delta\delta_N / \Delta\omega_N $	0.7	0.8	0.6		0.3	0.3	0.4	0.2	0.3	0.2	

^aThe errors in the values of $|\Delta\omega_N|$ are ± 0.1 ppm with the exception of those for Leu³⁵⁵ and Arg⁴⁶⁵ which are ± 0.2 ppm.

rapid transition on the submillisecond time scale between a major open ($\sim 97\%$) and a minor closed ($\sim 3\%$) state.¹⁴ Indeed, we have observed a close correspondence between the residue-specific ¹⁵N chemical shift differences ($\Delta\omega_N$) between the two states (as derived from analysis of the relaxation dispersion data) and the perturbations on the ¹⁵N chemical shifts ($\Delta\delta_N$) of EIC obtained from PEP titration experiments, indicating that the hydrogen bonds and salt bridges formed by the phosphoryl group of PEP with the side chains of Lys³⁴⁰, Arg³⁵⁸, and Arg⁴⁶⁵ effectively lock EIC in the closed conformation.¹⁴ Good agreement is also obtained by comparing the previously reported $\Delta\omega_N$ values for the open/closed conformational transition¹⁴ with the $\Delta\delta_N$ values measured upon α KG binding (Table 1), with discrepancies higher than 50% of the $\Delta\omega_N$ value observed only in the proximity of Lys³⁴⁰ (Figure 3c and Table 1). These observations indicate that α KG is not able to trap Lys³⁴⁰ in the closed conformation, and are fully consistent with our structural model of the EIC- α KG complex, in which the C⁵ carboxyl group of the inhibitor is involved in strong interactions with Arg³⁵⁸ and Arg⁴⁶⁵ but shows only minor contacts with the Lys³⁴⁰ side chain. This preferential orientation of the C⁵ carboxyl group is also confirmed by the small ¹H_N/¹⁵N chemical shift changes for Ile²⁷⁵ and Gly²⁷⁶ induced by α KG (Figure 1d), in contrast to the large perturbations observed upon addition of PEP (Figure 1d). The amide groups of Ile²⁷⁵ and Gly²⁷⁶ are indeed located close in space to the side chain of Arg²⁹⁶, which is involved in two hydrogen bonds with the PEP phosphoryl group but shows only minor contacts with α KG in the proposed structural model (Figure 3b,c). The absence of strong Arg²⁹⁶- α KG interactions leaves the Arg²⁹⁶ side chain with the same conformational flexibility as in the free protein. Consequently, the chemical environment of Ile²⁷⁵ and Gly²⁷⁶ is similar in both free EIC and the EIC- α KG complex, resulting in similar ¹H_N/¹⁵N chemical shifts (i.e., small $\Delta_{H/N}$ in Figure 1d).

As a final check of the proposed structural model, NMR titration experiments were performed to probe α KG binding to the EIC R465A mutant. Consistent with the disruption of two hydrogen bonds between the C⁵ carboxyl group of α KG and the Arg⁴⁶⁵ side chain, the K_D measured for the EIC R465A mutant- α KG complex ($\sim 6.7 \pm 0.4$ mM, Figure 5a) is ~ 3 times larger than that for the wild-type protein (Figure 1e). As expected, mutation of Arg⁴⁶⁵ also results in destabilization of the enzyme-PEP interaction, evidenced by the higher K_m value ($\sim 1.6 \pm 0.4$ mM) obtained for the EIC R465A mutant-PEP interaction from steady-state enzyme kinetic data (Figure 5b).

Concluding Remarks. Engineering microorganisms to synthesize bioderived molecules from renewable carbon sources has drawn increasing attention in recent years.^{16–18} In this context, the use of nitrogen-poor culture media has been shown to be advantageous to force carbon into pathways not needed for biomass production.^{10–12,19} For several practical applications, however, the mechanisms used by microorganisms to

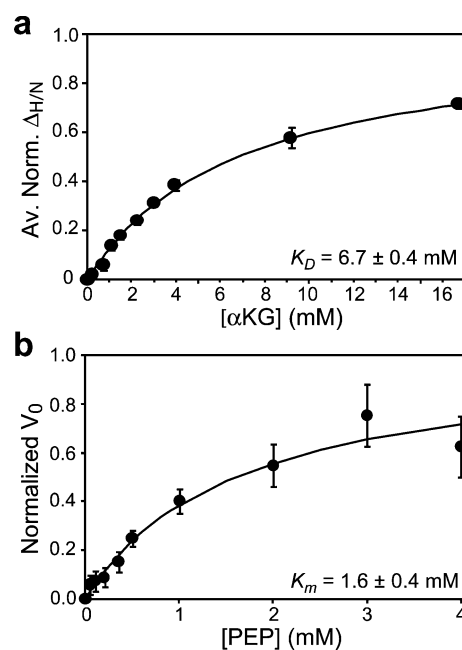


Figure 5. Effect of the active site R465A mutation on the binding of α KG and PEP to EIC. (a) Binding of α KG to the R465A EIC mutant as monitored by chemical shift perturbation. Data for all residues showing $\Delta_{H/N} > 0.1$ ppm at 16 mM α KG were simultaneously fit (solid curve) using a one-site binding model (see Methods). In the figure, the $\Delta_{H/N}$ were normalized with respect to the fitted $\Delta_{H/N}$ at saturation and averaged over all of the residues used in the fitting procedure. (b) Michaelis–Menten kinetics for the R465A EIC mutant with the substrate PEP in the absence of α KG. The error bars are set to one standard deviation.

balance nutrients run contrary to the metabolic engineer's goal of optimizing yields. Thus, in such cases, the use of new microorganisms in which carbon and nitrogen metabolism are uncoupled may be essential for maximizing production rates.

α KG provides the carbon substrate for the glutamine synthetase–glutamate synthase cycle, which assimilates ammonia to produce glutamate. Variations in the concentration of the nitrogen source in the growth medium result in rapid changes in the intracellular concentration of α KG from 0.5 to 10 mM when the nitrogen content of the medium is decreased sufficiently to limit cell growth.⁷ Interestingly, α KG has been shown in bacteria to link the rate of carbon uptake to the availability of a nitrogen source by inhibition of EI,⁷ providing an attractive system for synthetic biology studies aimed at engineering new microorganisms with uncoupled carbon and nitrogen metabolism.

Here, we have used NMR to investigate the interaction of α KG with *E. coli* EI. Analysis of the ¹H_N/¹⁵N chemical shift profiles generated by α KG on the NMR spectra of the isolated EIN and EIC domains (Figure 1a–d) clearly indicates that

```

EICNTR  AQLKSGERIKVMLNAGLSPEHEEKLGSRIDGIGLYRTEIPFMLQSGFPSEEEQVAQYQGM 486
EIC      AITLDGHQVEVCANIGTVRDVEGAERNGAEGVGLYRTEFLFMDRDALPTEEEQFAAYKAV 320
EICNTR  LQMFNDKPVTLRITLDVGADKQLPYMPTIS--EENPCLGWRGIRITLDQPEIFLIQVRAMLRA 545
EIC      AEACGSQAVIVRTMDIGGDKELPYMNFPEENPFLGWRRAIRIAMDRKEIILRDQLRAILRA 380
EICNTR  NAATGNLNIILPEMVTSLDEVDEARRLIERAGREVEEMIGYEIPKPRIGIMLEVPSMVFML 605
EIC      -SAFGKLRIMFPMIISVEEVRALRKEIEIYKQELRDEGKAFDESIEIGVMVETPAAATIA 439
EICNTR  PHLAKRVDFISVGTNDLTQYILAVDRNNTRVANIYDSLHPAMLRALAMIAREAEIHGIDL 665
EIC      RHLAKEVDFFSIGTNDLTQYTLAVDRGNDMISHLYQPMSPSVLNLIKQVIDASHAEKWT 499
EICNTR  RLCGEMAGDPMCVAAILIGLGYRHLMSNGRSVARAKYLLRRIDYAEAEENLAQRSLEAQLAT 725
EIC      GMCCELAGDERATLLLLGMGLDEFMSAISIPRIKKIIRNTNFEAKVLAEQALAQPTD 559
EICNTR  EVRHQVAAFMERRGMLIRGGL 748
EIC      ELMTLVNFIEEKTIC----- 575

```

Figure 6. Sequence alignment of EIC and the C-terminal domain of EI^{NTR} (EIC^{NTR}). The amino acid sequences of EIC and EIC^{NTR} were aligned in BLAST. Exactly conserved residues and conservative mutations are colored *green* and *blue*, respectively. EIC residues involved in the binding with PEP are colored in *red*.

α KG interacts exclusively with the C-terminal domain of EI at the binding site for PEP, thus acting as a competitive inhibitor of the enzyme. Although the segment Lys²⁵⁰-Pro²⁶⁰ was not included in either of the isolated domain constructs, this fragment comprises a helix connecting the N- and C-terminal domains of the enzyme, does not form pockets, and is not involved in any known interaction with PEP or other molecules. Therefore, the presence of an additional binding site for α KG in the Lys²⁵⁰-Pro²⁶⁰ fragment seems very unlikely.

Enzymatic assays performed in the absence and presence of α KG confirm the competitive nature of the inhibition (Figure 2a,b). The K_i of $\sim 2.2 \pm 0.5$ mM is in excellent agreement with the K_D of the EI- α KG complex measured by NMR titration experiments and indicates that under conditions of nitrogen limitation the enzyme-inhibitor interaction is strong enough to reduce the percentage of intracellular EI bound to PEP from 50% (at 0 mM α KG) to 15% (at 10 mM α KG) (Figure 2c). Although our results agree well with direct inhibition of EI by α KG, they are inconsistent with the non-competitive inhibition model previously proposed.⁷ In particular, Doucette et al.⁷ reported that addition of 2 mM α KG to a reaction mixture containing EI and PEP results in a $\sim 70\%$ reduction in the maximum velocity (V_{max}) for the EI autophosphorylation reaction. We note that in our first attempt to titrate α KG (SIGMA, product code 75892) into EIC we noticed the appearance of several new cross-peaks in the ¹H-¹⁵N TROSY spectrum of the protein (Supporting Information, Figure S2), indicative of protein degradation. The degradation was time-dependent, proceeded faster at higher concentrations of α KG (Supporting Information, Figure S2), and was not negligible under our experimental conditions (at 4 mM α KG the intensities of the EIC ¹H-¹⁵N cross-peaks dropped more than 60% after 20 min incubation at 37 °C). Similar effects were also observed upon titration α KG into the isolated EIN domain, suggesting that our batch of α KG contained a contaminant with high proteolytic activity. Protein degradation in subsequent experiments was eliminated by purchasing a new batch of α KG (SIGMA, product code K1875 Premium quality) that was resuspended in the working buffer at a final concentration of 100 mM, checked for pH, aliquoted, and immediately frozen. The use of a contaminated batch of α KG for the inhibition assay would result in a reduction in the concentration of active enzyme (that would be quickly proteolyzed by the contaminant) with a concomitant artificial decrease in V_{max} and may explain the discrepancy between our inhibition data and the ones previously reported.⁷ In this respect, we also note that although (i) the NMR data presented

here indicate unambiguously that α KG and PEP compete for the same binding site on EIC, (ii) the phosphoryl transfer reaction from PEP bound to the EIC domain to the active site histidine (His189) on the EIN domain is known to occur within the same subunit of the EI dimer,²⁰ and (iii) the structures of both free EI²² and a phosphoryl transfer intermediate of EI¹³ indicate that in-line phosphoryl transfer from EIC of one subunit to EIN of the second subunit within the dimer is sterically impossible, we cannot exclude that binding of α KG to one subunit may induce a conformational change in the relative orientations of the EIN and EIC domains of the second subunit that is incompetent for phosphoryl transfer. In such a case α KG could potentially act as both a competitive and non-competitive inhibitor of EI.

On the basis of the ¹H_N/¹⁵N chemical shift perturbation and enzymatic data that clearly indicated that α KG and PEP compete for the same binding site on EI, we built a model for the EIC- α KG complex by docking an α KG molecule into the binding site for PEP using the molecular docking program AutoDock. Our results indicate that the EIC- α KG complex retains most of the key interactions of the EIC-PEP complex (Figure 3), but with major differences observed at the C⁵ carboxyl group of α KG. In particular the inhibitor makes minimal contacts with the side chains of residues Arg²⁹⁶, Arg³³², and Lys³⁴⁰, which are involved in an extensive network of electrostatic interactions with the phosphoryl group of PEP. These observations are fully consistent with previously reported NMR relaxation dispersion data¹⁴ and are in good agreement with the effects induced by the inhibitor on the ¹H/¹⁵N chemical shifts (Figure 1d) and on the sedimentation coefficient of the enzyme (Figure 4), confirming that the structural model presented here is of good quality.

Though the competitive nature of the EI inhibition makes the design of EI mutants resistant to α KG nontrivial, the fact that the EIC residues involved in PEP binding are fully conserved in the enzyme EI^{NTR} (Figure 6), which catalyzes the same PEP-induced autophosphorylation reaction but is not inhibited by α KG,²¹ suggests that engineering such EI mutants is not an impossible task. In this respect, the EIC- α KG structure presented here may serve as model for structure-based protein design of EI/EI^{NTR} hybrids that maintain the same enzymatic activity of wild-type EI but are resistant to α KG.

METHODS

NMR Spectroscopy. The R465A mutant of EIC was created using the QuikChange Site-Directed Mutagenesis Kit (Stratagene). Intact *E. coli* EI (residues 1–575) and the isolated N-terminal (EIN, residues

1–249) and C-terminal (EIC, residues 261–575) domains were expressed and purified as described previously.^{14,22,23} All NMR samples were prepared in 20 mM Tris buffer, pH 7.4, 100 mM NaCl, 4 mM MgCl₂, 1 mM EDTA, 2 mM DTT, and 90% H₂O/10% D₂O (v/v). The protein concentration (in subunits) was 200–400 μM.

NMR spectra were recorded at 37 °C on Bruker 600 MHz spectrometers equipped with z-shielded gradient triple resonance cryoprobe. Spectra were processed using NMRPipe²⁴ and analyzed using the program SPARKY (<http://www.cgl.ucsf.edu/home/sparky>).

The ¹H–¹⁵N TROSY spectra of free EI and EIC were assigned according to previously reported NMR data.^{14,25} Assignment of the ¹H–¹⁵N cross-peaks for the EIC-αKG complex was performed by titration experiments, following the change in ¹H–¹⁵N cross-peak positions as a function of added αKG in ¹H–¹⁵N TROSY spectra.

Weighted combined ¹H/¹⁵N chemical shift perturbations (Δ_{H/N}) resulting from the addition of increasing concentrations of αKG (up to 16 mM) were calculated using the equation²⁶

$$\Delta_{H/N} = \sqrt{(\Delta\delta_H W_H)^2 + (\Delta\delta_N W_N)^2} \quad (1)$$

where W_H and W_N are weighting factors for the ¹H_N and ¹⁵N amide shifts, respectively ($W_H = 1$, $W_N = 0.154$), and $\Delta\delta_H$ and $\Delta\delta_N$ are the ¹H_N and ¹⁵N chemical shift differences in ppm, respectively, between free and bound states. The dissociation constant (K_D) for the EIC-αKG complex was obtained by fitting the changes in $\Delta_{H/N}$ with increasing concentration of αKG using the equation²⁷

$$\Delta_{H/N} = \Delta_0 \frac{P + L + K_D - \sqrt{(P + L + K_D)^2 - 4PL}}{2P} \quad (2)$$

where Δ_0 is the weighted combined ¹H/¹⁵N chemical shift at saturation, and P and L are the protein and ligand concentrations, respectively. The chemical shift perturbation curves of residues showing $\Delta_{H/N} > 0.1$ ppm in the presence of 16 mM αKG were simultaneously fitted to the same K_D value.

Backbone amide ¹D_{NH} residual dipolar couplings (RDCs) were measured by taking the difference in ¹J_{NH} scalar couplings in aligned and isotropic media.²⁸ The alignment media employed was phage *pf1* (14 mg mL⁻¹; ASLA Biotech),^{29,30} and ¹J_{NH} couplings were measured using the ARTSY pulse scheme.³¹

Enzymatic Assay. Enzymatic activity of EIC for the hydrolysis of PEP to inorganic phosphate and pyruvate was assayed spectrophotometrically in the presence of 0, 2, and 4 mM αKG. Assays were performed at 37 °C using the EnzChek Phosphate Assay Kit (Invitrogen) and a nanodrop 2000 spectrophotometer, as described previously.¹⁴ The experimental enzymatic velocities (ν) were fit using either a competitive or a non-competitive inhibition model describing the effect of αKG on the catalytic activity of EIC:

Competitive inhibition

$$\left\{ \begin{array}{l} \nu = \left(\frac{V_{\max}[\text{PEP}]}{K_m + [\text{PEP}]} \right), \quad \text{if } [\alpha\text{KG}] = 0 \\ \nu = \left(\frac{V_{\max}[\text{PEP}]}{K_m(1 + [\alpha\text{KG}]/K_I) + [\text{PEP}]} \right), \\ \quad \text{if } [\alpha\text{KG}] > 0 \end{array} \right. \quad (3)$$

Non-competitive inhibition

$$\left\{ \begin{array}{l} \nu = \left(\frac{V_{\max}[\text{PEP}]}{K_m + [\text{PEP}]} \right), \quad \text{if } [\alpha\text{KG}] = 0 \\ \nu = \left(\frac{V_{\max}[\text{PEP}]}{(1 + [\alpha\text{KG}]/K_I) + (K_m + [\text{PEP}])} \right), \\ \quad \text{if } [\alpha\text{KG}] > 0 \end{array} \right. \quad (4)$$

where K_m and V_{\max} are the Michaelis constant and maximum velocity in the absence of αKG, respectively, $[\text{PEP}]$ and $[\alpha\text{KG}]$ are the concentrations of PEP and αKG, respectively, and K_I is the inhibition constant.

The effective Michaelis constant for the EI-PEP complex ($K_{m,\text{eff}}$) at αKG concentrations ranging from 0 to 10 mM was calculated using the equation

$$K_{m,\text{eff}} = K_m(1 + [\alpha\text{KG}]/K_I) \quad (5)$$

K_m was set to 0.3 mM and K_I to 2.2 mM, as determined by the inhibition assay. The obtained $K_{m,\text{eff}}$ values were used to calculate the percentage of EI bound to PEP at physiological concentrations of enzyme (~10 μM subunits)³² and PEP (300 μM).³³ Results are presented in Figure 2c.

Docking Calculations. The binding mode of αKG to EIC was modeled by docking simulations using the program Autodock 4.0.³⁴ The coordinates of the C-terminal domain from the phosphorylated EI X-ray structure¹³ were used as the target in the docking calculations. A cubic grid box (grid spacing = 0.373 Å; 40 × 40 × 40 grid points) centered on the coordinates of the phosphorylated His¹⁸⁹ phosphorus atom was used, and the grid maps were generated using the program Autogrid. Docking was performed using the Lamarckian genetic algorithm (LGA) and allowing the side chains of Arg³³² and Cys⁵⁰² conformational flexibility during the simulations. For αKG, the acrylic and carboxylic group were considered rigid, and only the bonds involving the two sp³ carbons were treated as rotatable; 100 runs were performed. The population size was set to 150, the maximum number of evaluations to 2,500,000, and the maximum number of generations to 27,000. The remaining parameters were set to their default values. Out of the 100 structures generated, the 10 lowest energy conformations display the same ligand orientation in the binding site. The conformation with the lowest binding energy is displayed in Figure 3c.

Sedimentation Velocity. A 1.5 mM stock solution of uniformly ²H/¹⁵N-labeled EI was diluted to prepare a series of solutions of approximately 130, 65, and 32 μM in 100 mM NaCl, 20 mM Tris buffer, pH 7.4, 4 mM MgCl₂, 2 mM DTT, and 1 mM EDTA (buffer A). The lowest concentration solution was serially diluted into the same buffer to prepare approximately 2–16 μM solutions. All samples were analyzed by sedimentation velocity at 20.0 °C and 50 krpm on a Beckman Coulter ProteomeLab XL-I analytical ultracentrifuge. Dilute protein solutions (<50 μM) were loaded into 12 mm 2-channel Epon centerpiece cells (400 μL), whereas higher concentrations were loaded into 3 mm 2-channel Epon centerpiece cells (100 μL). Absorbance (280 nm) and Rayleigh interference (655 nm) scans collected at approximately 7 min intervals were analyzed in SEDFIT 13.0d³⁵ in terms of a continuous $c(s)$ distribution covering an s range of 0.0–10.0 S with a resolution of 200 and a confidence level of 0.68. Good fits were obtained with rmsd values corresponding to typical instrumental noise values. Identical experiments were carried out in buffer A containing 20 mM PEP (buffer B) or 20 mM αKG (buffer C). The solution density (ρ) and viscosity (η) for buffer A were calculated on the basis of the solvent composition using SEDNTERP 1.09.³⁶ Solution densities for buffers B and C were measured at 20.000 °C on an Anton-Paar DMA 5000 density meter; solution viscosities were measured at 20.00 °C using an Anton Paar AMVn rolling ball viscometer. The partial specific volume for EI (ν) was calculated in SEDNTERP 1.09³⁶ and adjusted for its isotopic composition.

EI monomer and dimer populations obtained from integration of the $c(s)$ distributions were used to construct partial concentration isotherms. Data were analyzed in SEDPHAT 10.41³⁷ in terms of a monomer–dimer self-association to obtain the equilibrium constants; errors were determined using the method of F-statistics with a confidence level of 95%.

■ ASSOCIATED CONTENT

■ Supporting Information

Analytical ultracentrifugation data for Enzyme I in the presence of phosphoenolpyruvate and α -ketoglutarate, and ^1H - ^{15}N TROSY correlation spectra of Enzyme I in the presence of various concentrations of α -ketoglutarate. This material is available free of charge via the Internet at <http://pubs.acs.org>

■ AUTHOR INFORMATION

Corresponding Author

*E-mail: mariusc@mail.nih.gov.

Notes

The authors declare no competing financial interest.

■ ACKNOWLEDGMENTS

We thank N. Fawzi and Y. Takayama for helpful discussions. This work was supported by funds from the Intramural Program of the NIH, NIDDK, and the Intramural AIDS Targeted Antiviral Program of the Office of the Director of the NIH (to G.M.C.).

■ REFERENCES

- (1) Guertin, D. A., and Sabatini, D. M. (2007) Defining the role of mTOR in cancer. *Cancer Cell* 12, 9–22.
- (2) Kapahi, P., Chen, D., Rogers, A. N., Katewa, S. D., Li, P. W., Thomas, E. L., and Kockel, L. (2010) With TOR, less is more: a key role for the conserved nutrient-sensing TOR pathway in aging. *Cell Metab.* 11, 453–465.
- (3) Anderson, A. J., and Dawes, E. A. (1990) Occurrence, metabolism, metabolic role, and industrial uses of bacterial polyhydroxyalkanoates. *Microbiol. Rev.* 54, 450–472.
- (4) Wargacki, A. J., Leonard, E., Win, M. N., Regitsky, D. D., Santos, C. N., Kim, P. B., Cooper, S. R., Raisner, R. M., Herman, A., Sivitz, A. B., Lakshmanaswamy, A., Kashiyama, Y., Baker, D., and Yoshikuni, Y. (2012) An engineered microbial platform for direct biofuel production from brown macroalgae. *Science* 335, 308–313.
- (5) Dellomonaco, C., Clomburg, J. M., Miller, E. N., and Gonzalez, R. (2011) Engineered reversal of the beta-oxidation cycle for the synthesis of fuels and chemicals. *Nature* 476, 355–359.
- (6) Bokinsky, G., Peralta-Yahya, P. P., George, A., Holmes, B. M., Steen, E. J., Dietrich, J., Soon Lee, T., Tullman-Ercek, D., Voigt, C. A., Simmons, B. A., and Keasling, J. D. (2011) Synthesis of three advanced biofuels from ionic liquid-pretreated switchgrass using engineered *Escherichia coli*. *Proc. Natl. Acad. Sci. U.S.A.* 108, 19949–19954.
- (7) Doucette, C. D., Schwab, D. J., Wingreen, N. S., and Rabinowitz, J. D. (2011) α -Ketoglutarate coordinates carbon and nitrogen utilization via enzyme I inhibition. *Nat. Chem. Biol.* 7, 894–901.
- (8) Boer, V. M., Crutchfield, C. A., Bradley, P. H., Botstein, D., and Rabinowitz, J. D. (2010) Growth-limiting intracellular metabolites in yeast growing under diverse nutrient limitations. *Mol. Biol. Cell* 21, 198–211.
- (9) Meadow, N. D., Fox, D. K., and Roseman, S. (1990) The bacterial phosphoenolpyruvate:glucose phosphotransferase system. *Annu. Rev. Biochem.* 59, 497–542.
- (10) Monot, F., and Engasser, J. M. (1983) Production of acetone and butanol by batch and continuous culture of *Clostridium acetobutylicum* under nitrogen limitation. *Biotechnol. Lett.* 5, 213–218.
- (11) Kessler, B., Weusthuis, R., Witholt, B., and Eggink, G. (2001) Production of microbial polyesters: fermentation and downstream processes. *Adv. Biochem. Eng. Biotechnol.* 71, 159–182.
- (12) Aoyama, K., Uemura, I., Miyake, J., and Asada, Y. (1997) Fermentative metabolism to produce hydrogen gas and organic compounds in a cyanobacterium, *Spirulina platensis*. *J. Ferment. Bioeng.* 83, 17–20.
- (13) Teplyakov, A., Lim, K., Zhu, P. P., Kapadia, G., Chen, C. C., Schwartz, J., Howard, A., Reddy, P. T., Peterkofsky, A., and Herzberg, O. (2006) Structure of phosphorylated enzyme I, the phosphoenolpyruvate:sugar phosphotransferase system sugar translocation signal protein. *Proc. Natl. Acad. Sci. U.S.A.* 103, 16218–16223.
- (14) Venditti, V., and Clore, G. M. (2012) Conformational selection and substrate binding regulate the monomer/dimer equilibrium of the C-terminal domain of *Escherichia coli* Enzyme I. *J. Biol. Chem.* 287, 26989–26998.
- (15) Patel, H. V., Vyas, K. A., Savtchenko, R., and Roseman, S. (2006) The monomer/dimer transition of enzyme I of the *Escherichia coli* phosphotransferase system. *J. Biol. Chem.* 281, 17570–17578.
- (16) Steen, E. J., Kang, Y., Bokinsky, G., Hu, Z., Schirmer, A., McClure, A., Del Cardayre, S. B., and Keasling, J. D. (2010) Microbial production of fatty-acid-derived fuels and chemicals from plant biomass. *Nature* 463, 559–562.
- (17) Schirmer, A., Rude, M. A., Li, X., Popova, E., and del Cardayre, S. B. (2010) Microbial biosynthesis of alkanes. *Science* 329, 559–562.
- (18) Causey, T. B., Zhou, S., Shanmugam, K. T., and Ingram, L. O. (2003) Engineering the metabolism of *Escherichia coli* W3110 for the conversion of sugar to redox-neutral and oxidized products: homoacetate production. *Proc. Natl. Acad. Sci. U.S.A.* 100, 825–832.
- (19) Illman, A. M., Scragg, A. H., and Shales, S. W. (2000) Increase in *Chlorella* strains calorific values when grown in low nitrogen medium. *Enzyme Microb. Technol.* 27, 631–635.
- (20) Navdaeva, V., Zurbriggen, A., Waltersperger, S., Schneider, P., Oberholzer, A. E., Bahler, P., Bachler, C., Grieder, A., Baumann, U., and Erni, B. (2011) Phosphoenolpyruvate: sugar phosphotransferase system from the hyperthermophilic *Thermoanaerobacter tengcongensis*. *Biochemistry* 50, 1184–1193.
- (21) Rabus, R., Reizer, J., Paulsen, I., and Saier, M. H. (1999) Enzyme INtr from *Escherichia coli*. *J. Biol. Chem.* 274, 26185–26191.
- (22) Schwieters, C. D., Suh, J. Y., Grishaev, A., Ghirlando, R., Takayama, Y., and Clore, G. M. (2010) Solution structure of the 128 kDa enzyme I dimer from *Escherichia coli* and its 146 kDa complex with HPr using residual dipolar couplings and small- and wide-angle X-ray scattering. *J. Am. Chem. Soc.* 132, 13026–13045.
- (23) Suh, J. Y., Cai, M., and Clore, G. M. (2008) Impact of phosphorylation on structure and thermodynamics of the interaction between the N-terminal domain of enzyme I and the histidine phosphocarrier protein of the bacterial phosphotransferase system. *J. Biol. Chem.* 283, 18980–18989.
- (24) Delaglio, F., Grzesiek, S., Vuister, G. W., Zhu, G., Pfeifer, J., and Bax, A. (1995) NMRPipe: a multidimensional spectral processing system based on UNIX pipes. *J. Biomol. NMR* 6, 277–293.
- (25) Garrett, D. S., Seok, Y. J., Liao, D. I., Peterkofsky, A., Gronenborn, A. M., and Clore, G. M. (1997) Solution structure of the 30 kDa N-terminal domain of enzyme I of the *Escherichia coli* phosphoenolpyruvate:sugar phosphotransferase system by multidimensional NMR. *Biochemistry* 36, 2517–2530.
- (26) Mulder, F. A., Schipper, D., Bott, R., and Boelens, R. (1999) Altered flexibility in the substrate-binding site of related native and engineered high-alkaline *Bacillus subtilis*. *J. Mol. Biol.* 292, 111–123.
- (27) Granot, J. (1983) Determination of dissociation constants of 1:1 complexes from NMR data. Optimization of the experimental setup by statistical analysis of simulated experiments. *J. Magn. Reson.* 55, 216–224.
- (28) Bax, A., Kontaxis, G., and Tjandra, N. (2001) Dipolar couplings in macromolecular structure determination. *Methods Enzymol.* 339, 127–174.
- (29) Clore, G. M., Starich, M. R., and Gronenborn, A. M. (1998) Measurement of residual dipolar couplings of macromolecules aligned in the nematic phase of a colloidal suspension of rod-shaped viruses. *J. Am. Chem. Soc.* 120, 10571–10572.
- (30) Hansen, M. R., Mueller, L., and Pardi, A. (1998) Tunable alignment of macromolecules by filamentous phage yields dipolar coupling interactions. *Nat. Struct. Biol.* 5, 1065–1074.
- (31) Fitzkee, N. C., and Bax, A. (2011) Facile measurement of ^1H - ^{15}N residual dipolar couplings in larger perdeuterated proteins. *J. Biomol. NMR* 48, 65–70.

- (32) Rohwer, J. M., Meadow, N. D., Roseman, S., Westerhoff, H. V., and Postma, P. W. (2000) Understanding glucose transport by the bacterial phosphoenolpyruvate:glycose phosphotransferase system on the basis of kinetic measurements *in vitro*. *J. Biol. Chem.* 275, 34909–34921.
- (33) Albe, K. R., Butler, M. H., and Wright, B. E. (1990) Cellular concentrations of enzymes and their substrates. *J. Theor. Biol.* 143, 163–195.
- (34) Morris, G. M., Huey, R., Lindstrom, W., Sanner, M. F., Belew, R. K., Goodsell, D. S., and Olson, A. J. (2009) AutoDock4 and AutoDockTools4: Automated docking with selective receptor flexibility. *J. Comput. Chem.* 30, 2785–2791.
- (35) Schuck, P. (2000) Size-distribution analysis of macromolecules by sedimentation velocity ultracentrifugation and Lamm equation modeling. *Biophys. J.* 78, 1606–1619.
- (36) Cole, J. L., Lary, J. W., T, P. M., and Laue, T. M. (2008) Analytical ultracentrifugation: sedimentation velocity and sedimentation equilibrium. *Methods Cell Biol.* 84, 143–179.
- (37) Schuck, P. (2003) On the analysis of protein self-association by sedimentation velocity analytical ultracentrifugation. *Anal. Biochem.* 320, 104–124.